Synthesis, characterization and comparative gas sensing study of ZnO–GO and ZnO–rGO compounds

Nastaran Sadat Hosseini
Takestan Islamic Azad University
javad Hassanzadeh (javadhasanzadeh1649@gmail.com)
Takestan Islamic Azad University
Ali Abdolahzadeh Ziabari
Islamic Azad University of Lahijan

Research Article

Keywords: Gas–sensor, Graphene, ZnO, Ethanol, Recovery time, Sensitivity

Posted Date: January 18th, 2022

DOI: https://doi.org/10.21203/rs.3.rs-1239473/v1

Abstract

In this work, we prepare composites of ZnO–GO and ZnO–rGO through an economic and facile route and comparatively study their gas sensitivity towards ethanol. The morphological, compositional and structural properties of the prepared composites are investigated using scanning electron microscopy (SEM), energy–dispersive X–ray (EDX) spectroscopy, and X–ray diffraction (XRD) analysis. The optimal work temperature of 300˚C was observed for the prepared samples. ZnO–GO–based sensor shows higher sensitivity than ZnO–rGO. Also, the variation of response and recovery time with the gas concentration is investigated. As is expected, the sensitivity increases as the gas concentration increases. Besides, it was revealed that the response and recovery time is a function of the surface morphology.

1. Introduction

Gas sensors are employed for detection of toxic, diffuse and combustible gases. These devices are also extensively utilized in industry and in firefighting. Various types of materials have been studied to fabricate gas sensors, such as optical fibers [1], inorganic semiconductors [2], polymers [3], and carbon nanomaterials [4]. Graphene has attracted lots of attentions as a gas sensing material since 2004 when it was discovered. It shows high specific area (2630 m^2/g), high mobility of 20,000 $cm^2/$ V.s at room temperature, highest surface to volume ratio among the known layered materials and low electrical noise [5]. Amongst graphene compounds, graphene oxide (GO) is an electrical insulator mainly due to pendent oxygen functional groups that restrict it for gas sensing. The conductivity of GO can be restored close to graphene by elimination of oxygen functional groups and restoration of aromatic double bonded carbons through chemical reduction or high temperature heat treatment [6, 7]. The process of reduction has a remarkable effect on how close reduced GO (rGO) is achieved, in terms of structure, to porous graphene (PG) and its quality. Compared to PG, rGO has shown promising properties in detection of different gases regarding its low production cost, fine tuning structure, dispersibility to water, feasibility of further modification, premium electrical conductivity and chemically active defect sites [6].Many efforts have been carried out to increase the gas sensing of rGO such as hybridization with metal oxides, polymers and functionalizing with different chemical groups [8, 9]. Recently, hybrid structure of rGO and metal oxide semiconductor (MOS) structures have been investigated for highly sensitive, selective and economic gas sensors that work at low temperature [5]. Nanostructured MOSs such as ZnO, SnO_2, and Cu_2O, are widely used in gas sensing devices due to their high specific surface area, large aspect ratio, and good flexibility. However, these nanostructures have poor electrical conductivity. The hybridization of MOSs with two–dimensional graphene can effectively improve their electrical conductivity and improve their sensing performance. ZnO is extensively used in a wide range of applications, including gas sensors, transparent electrodes, optoelectronic devices, etc [10]. ZnO–based gas sensors usually work at temperature range of 200–450°C [11]. Working at high temperature increases the redox reactions underlying the sensing mechanism of chemiresitors. Hence, reduction of the working temperature is crucial in fabrication of low power consumption and small size chemical sensors. In this study, we report the synthesis and characterization of nanoparticle composites of rGO–ZnO and GO–ZnO through a

facile and low cost method. The aim is to perform a comparative study of the gas sensing capability of the produced composites which is scarce in the literature. The sensing traits of the achieved compounds have been analyzed toward ethanol gas at different work temperature and gas concentration.

2. Experimental Details

Initially, 1 mg of graphene oxide was dissolved in 15 ml isopropanol using an ultrasonic bath for 1.5 h. Then, to prepare the ZnO solution, 2.6 g of zinc acetate was dissolved into 30 ml ethanol and stirred at 70 ° C for 2 h. During the stirring, diethanolamine as the stabilizer was added to the solution until a transparent solution was obtained. The yielded solution containing the graphene oxide then was centrifuged for 4 minutes at 4,000 rpm. After centrifugation, the sediment phase was removed and the left homogenous solution was kept for the next step. 10 ml of graphene oxide solution then was mixed with 20 ml of zinc acetate solution and the obtained mixture was placed in an ultrasonic bath for 1h.This solution then was used for preparation of thin films by dip–coating method. Before dip–coating, the soda lime substrates were initially degreased by detergent and washed thoroughly by deionized water. To remove the macroscopic contaminations, the substrates were cleaned ultrasonically in a surfactant containing ethanol and acetone (each of 50% in volume). The cleaned substrates were dipped into the prepared solution and withdrawn from it vertically at a speed of 116 mm/min. The coated glass substrate was then dried at 150°C for 10 min in an oven to evaporate the solvent and organic residuals. This procedure was repeated 20 times. The dried thin films then were post annealed in air at 450 ° C for 1 h. The powder samples were also prepared from the solution used for thin film deposition. Exact the same procedure was followed to prepare a composition of reduced graphene oxide and zinc oxide. Finally, two types of compounds including GO–ZnO and rGO–ZnO, both in the form of thin films were prepared.

3. Characterization

The structure of the prepared thin films was studied by the X–ray diffraction (XRD) method using a (Panalytical X'PERT PRO) with CuK_a radiation (λ = 0.15406 nm). Surface morphology of the films was studied by field effect scanning electron microscopy (FESEM) with a (MIRA3, TESCAN) instrument equipped with Energy–dispersive X–ray spectroscopy (EDX) for surface chemical compositions analysis. Gas sensing analysis of the samples toward ethanol injection was carried out by a homemade static system [12]. The response of the device for reducing gas is determined as [13]

$$S = \frac{R_a(\Omega)}{R_g(\Omega)} = \frac{\left(\frac{V_C(V)}{V_{Ra}(V)} - 1\right)}{\left(\frac{V_C(V)}{V_{Rg}(V)} - 1\right)} \qquad (1)$$

where R_a and R_g are the baseline resistance of the sensing film in pure air and in a gas environment, respectively. V_{Rg} and V_{Ra} denote the voltages of variable resistor with and without ethanol ambient,

respectively. The response time is the time taken for the sample resistance to reach 90% of the equilibrium value after injection of the test gas. The recovery time is defined as the required time for the sample to return to 10% of its original resistance in air after removal of the test gas.

4. Results And Discussion

Figure 1 displays the XRD pattern of the prepared ZnO–GO and ZnO–rGO thin films. The diffraction peaks show the reflections (100), (002), (101), (102), (110), (103), (200), (112) and(201) of ZnO in a hexagonal Wurtzite lattice which agree with JCPDS No. 36–1451 of ZnO [14].

The lack of any secondary phase approves the synthesis of single phase ZnO nanocrystals. The average crystallite size of the samples was evaluated by Scherrer's equation [15]

$$D = \frac{0.9\lambda}{\beta \cos\theta} \qquad (2)$$

where β is the full–width at half maximum (FWHM) of the peak (in radians), θ is the Bragg's diffraction angle at the peak position and λ is the wavelength of the X–ray radiation.

The average crystallite size for GO–ZnO and rGO–ZnO nanocomposite was found 85 and 20 nm, respectively. As it is obvious from Fig. 1, no diffraction peak related to GO and rGO is observed. It can be due to: (1) lesser amount, giving relatively low diffraction intensity of GO and rGO than ZnO in the synthesized nanocomposite and (2) anchoring of ZnO nanoparticles on GO and rGO might hinder the restacking of carbon sheets, which leads to weak diffraction peak or no diffraction peak at all [16, 17].

Figure 2 demonstrates the back scattered electron SEM (BE–SEM) morphology and EDX mappings of localized microstructure in GO– and rGO–ZnO thin films. It confirms that Zn, O and C are the main elements in the samples. The results have been shown quantitively in Fig. 3 and Table 1.

The following figure shows the SEM results of the films.

Table 1
Quantitative analysis of structure based on GO/rGO–ZnO.

Elt	Line	Int.	Error	W%	A%
C	K_α	9.2/9.5	20.36/11.97	5.71/6.27	12.24/9.14
O	K_α	347.3/496.6	21.04/12.37	41.67/79.58	67.04/87.07
Zn	K_α	154.4/20.9	0.53/0.51	52.62/14.15	20.72/3.79
				100.00	100.00

To investigate the influence of GO and rGO on the nanoparticle distribution on the samples, FESEM analyses of GO–ZnO and rGO–ZnO were performed .Fig. 4 shows the microstructure of GO– and rGO–ZnO thin films at different magnifications. The FESEM images clearly show the hexagonal agglomeration of GO–ZnO nanoparticles with the average size of 90 nm and the spherical rGO–ZnO nanoparticles with average size of 20 nm. As observed in Fig. 4, the presence of rGO significantly affects the size distribution and morphology of the nanoparticles. Obviously, finer nanoparticles distributed on a less porous morphology are seen. A more careful and closer–up view reveals that the individual rGO–ZnO nanoparticles with the size of 20 nm are well separated from each other and are well distributed on the surface.

The gas sensitivity of the prepared thin films was analyzed by exposure the samples to ethanol vapor. The variation of the resistance of the prepared thin films was monitored through the measurement of the voltage of a variable resistor. By adsorption and desorption of oxygen on the surface of MOSs the electrical resistance changes. The MOS thin film adsorbs the oxygen molecules as is exposed to the air. The adsorption increases as the temperature increases and the adsorbed oxygen molecules oxidize the surface MOSs. Consequently, O^{2-} ions emerge that lead to increase of the sensor resistance. When ethanol is introduced, a reaction between oxygen ions and the adsorbed ethanol molecules occurs which releases electrons back to the conduction band followed by decrease in the sensor resistance. Because almost all MOS gas sensors have no good response at room temperature, finding an optimal operating temperature is a main problem. Fortunately, the synergistic effects of ZnO doped with graphene have drastically improved the sensitivity of ZnO gas sensors [19]. It is believed that the combination of ZnO with functionalized graphene is a promising remedy for development of ZnO–based gas sensors with low working temperatures and high sensitivity [20]. We followed this solution for improvement of the performance of the prepared ZnO gas sensors.

The sensitivity of the thin films under injection of 1200 ppm ethanol is displayed in Fig. 5. As can be observed, the working temperature for both samples is the same at 300˚C. When compared to the reported values for pure ZnO thin film prepared by the same method and conditions [18], it seems very promising.

From Fig. 5, after the optimal temperature, the sensitivity decreased drastically. Commonly, this trend is linked to the gas adsorption/desorption events on the surface of the sensor. When the working temperature is low, the required thermal energy to overcome the activation energy barrier is not enough and no reaction with the absorbed oxygen occurs. When the temperature increases, sufficient O^{2-} molecules present on the surface to react with ethanol vapor molecules. Accordingly, an improvement in the sensor performance is observed. At temperatures higher than the optimal value, the performance is deteriorated mainly owing to less adsorbed O^{2-} compared to the desorbed O^{2-} as well as evaporation of ethanol molecules before reaction.

The time of the response ($T_{res.}$) and recovery ($T_{rec.}$) are key factors to determine the performance of the gas sensor. T_{res} is the time when the resistance reaches stability after the injection of the gas, while $T_{rec.}$

is the time when the resistance reaches 90% of the initial value in the air. The real–time dynamic response curve of the ZnO–GO and ZnO–rGO to 1200 ppm ethanol gas at 13 V is depicted in Fig. 6. One can see that $T_{res.}$= 64 s and the $T_{rec.}$= 120 s for ZnO–GO and $T_{res.}$= 13 s and the $T_{rec.}$= 35 s for ZnO–rGO. The reason of the observed difference between the response time of ZnO–GO and ZnO–rGO can be mainly assigned to the slower speed of the adsorption and desorption of ethanol, and more porosity of ZnO–GO thin film, which operates as reaction centers to compel oxygen and ethanol molecules to stay long enough to perform the gas–sensing reaction.

The performance of a gas sensor is a function of the gas concentration. When the gas concentration is low, the interaction probability decreases. At higher gas concentrations, more gas molecules interact with the chemisorbed oxygen molecules leading to more intense response. Fig. 7 depicts the real–time dynamic response of ZnO–GO and ZnO–rGO thin films upon exposure to different concentration of ethanol at 300˚C. As illustrated in Fig. 7a and b, the curve rises as the ethanol vapor is injected into the test system and declines rapidly when the ethanol vapor is released. The response amplitude of the thin films gradually grows when the gas concentration increases from 600 to 1680 ppm. The response and recovery properties of ZnO–GO and ZnO–rGO thin films are approximately reproducible, which implies the stability of the response of the prepared thin films. Those are critical features for the commercial application of any electronic devices. The calculated sensitivity of the samples as a function of the gas concentration is shown in Fig. 7c. It is clear that, the sensitivity of both ZnO–GO and ZnO–rGO thin films increases with the ethanol vapor concentration. Also, the sensing characteristics related to ZnO–GO thin film seems more appropriate than ZnO–rGO in detection of ethanol.

5. Conclusion

In summary, ZnO–GO and ZnO–rGO thin films were successfully grown by a facile and economic method. The pertinent structural, morphological, compositional and gas sensing properties of the films were studied in details. The structural measurement showed a wurtzite hexagonal structure related to polycrystalline ZnO. The morphological features of the samples revealed evenly distributed nanograins on the surface of the films. The compositional measurement confirmed the presence of Zn, O and C in the compounds. The samples showed an appropriate sensitivity towards ethanol gas. Especially, the working temperature of ZnO–based gas sensor improved as ZnO was alloyed with GO and rGO. We achieved the promising work temperature of 300˚C for the synthesized thin films. The dynamic response and recovery characteristics of the films were studied comparatively. Results show that the prepared ZnO–GO thin film can be a very good candidate for ethanol gas sensors.

Declarations

Acknowledgment

All authors would like to thank Dr. Abbas Bagheri Khatibani for his helpful advice on various technical issues examined in this paper.

Author declaration

[Instructions: Please check all applicable boxes and provide additional information as requested.]

1. Conflict of Interest

☐Potential conflict of interest exists:

We wish to draw the attention of the Editor to the following facts, which may be considered as potential conflicts of interest, and to significant financial contributions to this work:

The nature of potential conflict of interest is described below:

☐No conflict of interest exists.

We wish to confirm that there are no known conflicts of interest associated with this publication and there has been no significant financial support for this work that could have influenced its outcome.

2. Funding

☐Funding was received for this work.

All of the sources of funding for the work described in this publication are acknowledged below:

[List funding sources and their role in study design, data analysis, and result interpretation]

☐No funding was received for this work.

3. Intellectual Property

☐We confirm that we have given due consideration to the protection of intellectual property associated with this work and that there are no impediments to publication, including the timing of publication, with respect to intellectual property. In so doing we confirm that we have followed the regulations of our institutions concerning intellectual property.

4. Research Ethics

☐We further confirm that any aspect of the work covered in this manuscript that has involved human patients has been conducted with the ethical approval of all relevant bodies and that such approvals are acknowledged within the manuscript.

☐IRB approval was obtained (required for studies and series of 3 or more cases)

☐Written consent to publish potentially identifying information, such as details or the case and photographs, was obtained from the patient(s) or their legal guardian(s).

5. Authorship

The International Committee of Medical Journal Editors (ICMJE) recommends that authorship be based on the following four criteria:

1. Substantial contributions to the conception or design of the work, or the acquisition, analysis, or interpretation of data for the work, AND
2. Drafting the work or revising it critically for important intellectual content, AND
3. Final approval of the version to be published, AND
4. Agreement to be accountable for all aspects of the work in ensuring that questions related to the accuracy or integrity of any part of the work are appropriately investigated and resolved.

All those designated as authors should meet all four criteria for authorship, and all who meet the four criteria should be identified as authors. For more information on authorship, please see http://www.icmje.org/recommendations/browse/roles-and-responsibilities/defining-the-role-of-authors-and-contributors.html#two.

☐All listed authors meet the ICMJE criteria. ☒We attest that all authors contributed significantly to the creation of this manuscript, each having fulfilled criteria as established by the ICMJE.

☐One or more listed authors do(es) not meet the ICMJE criteria.

We believe these individuals should be listed as authors because:

[Please elaborate below] ☒

☐We confirm that the manuscript has been read and approved by all named authors.

☐We confirm that the order of authors listed in the manuscript has been approved by all named authors.

6. Contact with the Editorial Office

The Corresponding Author declared on the title page of the manuscript is:

Javad Hassanzadeh

☐This author submitted this manuscript using his/her account in EVISE.

☐We understand that this Corresponding Author is the sole contact for the Editorial process (including EVISE and direct communications with the office). He/she is responsible for communicating with the other authors about progress, submissions of revisions and final approval of proofs.

☐We confirm that the email address shown below is accessible by the Corresponding Author, is the address to which Corresponding Author's EVISE account is linked, and has been configured to accept

email from the editorial office of American Journal of Ophthalmology Case Reports:

☐Someone other than the Corresponding Author declared above submitted this manuscript from his/her account in EVISE:

[Insert name below]

☐We understand that this author is the sole contact for the Editorial process (including EVISE and direct communications with the office). He/she is responsible for communicating with the other authors, including the Corresponding Author, about progress, submissions of revisions and final approval of proofs.

References

1. W. H. Chua, M. H. Yaacob, C. Y. Tan, B. H. Ong, Chemical bath deposition of h–MoO_3 on optical fiber as room–temperature ammonia gas sensor, Ceramics International, 47(23) (2021) 32828–32836.
2. A. Bagheri Khatibani, A. AbdolahzadehZiabari, S. M. Rozati, Z. Bargbidi, G. Kiriakidis, Characterization and gas–sensing performance of spray pyrolyzed In_2O_3 thin films: substrate temperature effect, Transaction on Electrical and Electronic Materials, 13(3) (2012) 111–115.
3. M. Hao, R. Zhang, X. Jia, X. Gao, W. Gao, L. Cheng, Y. Qin, A polymer based self–powered ethanol gas sensor to eliminate the interreference of ultraviolet light, Sensors and Actuators A: Physical, 332(2) (2021) 113173.
4. H. T. Hussein, M. H. Kareem, A. M. Abdul Hussein, Synthesis and Characterization of carbon nanotube doped with zinc oxide nanoparticles CNTs–ZnO/PS as ethanol gas sensor, Optik, 248 (2021) 168107.
5. N. B. Thakare, F. C. Raghuwanshi, V. S. Kalyamwar, Y. S. Tamgadge, Reduced graphene oxide–ZnOcomposites based gas sensors: A review, AIP Conference Proceedings, 1953 (2018) 030057.
6. F. Yavari, N. Koratkar, Graphene–based chemical sensors, J. Phys. Chem. Lett. 3(13) (2012) 1746–1753.
7. A. Lipatov, A. Varezhnikov, P. Wilson, V. Seysoev, A. Kolmakov, A. Sinitskii, Highly selective gas sensor arrays based on thermally reduced graphene oxide, 5(12) (2013) 5426–5434.
8. F.–L. Meng, Z. Guo, X. –J. Huang, Graphene–based hybrids for chemiresistive gas sensors, TrAC Trends in Analytical Chemistry, 68 (2015) 37–47.
9. W. Yuan, G. Shi, Graphene–based gas sensors, Journal of Materials Chemistry A, 1(35) (2013) 10078–10091.
10. K. Ahmadi, A. AbdolahzadehZiabari, K. Mirabbaszadeh, A. Ahadpour Shal, Synthesis and characterization of ZnO/TiO_2 composite core/shell nanorod arrays by sol–gel method for organic solar cell applications, Bulletin of Materials Science, 38 (2015) 617–623.

11. M. J. S. Spencer, Gas sensing applications of 1D–nanostructured zinc oxide: Insights from density functional theory calculations, Progress inMaterials Science 57 (2012) 437–486.
12. A. Bagheri Khatibani, M. Abbasi, Effect of Fe and Co doping on ethanol sensing property of powder–based ZnO nanostructures prepared by sol–gel method**,** J. Sol–Gel Sci. Technol. 86 (2018) 255–265.
13. A. Bagheri Khatibani, Characterization and ethanol sensing performance of sol–gel derived pure and doped zinc oxide thin films, Journal of Electronic Materials 48 (2019) 3784–3793.
14. Joint Committee on Powder Diffraction, Powder Diffraction File, Card 36–1451(ZnO), (ICDD, Swarthmore, PA, 1996)
15. A. Abdolahzadeh Ziabari, N. M. Zindanlou, J. Hassanzadeh, S. Golshahi, A. B. Khatibani, Fabrication and study of single–phase high–hole–mobility CZTS thin films for PV solar cell applications: Influence of stabilizer and thickness, J. Alloy Compd. 842 (2020) 155741.
16. [16] C. Xu, X. Wang, J. Zhu, Graphene–metal nanoparticle composites, J. Phys. Chem. C, 112 (2008) 19841–19845.
17. X. Liu, L. Pan, Q. Zhao, T. Lv, G. Zhu, T. Chen, T. Lu, Z. Sun, C. Sun,UV–assisted photocatalytic synthesis of ZnO–reduced graphene oxide composites with enhanced photocatalytic activity in reduction of Cr(VI), Chem. Eng. J.183 (2012) 238–243.
18. A. B. Khatibani, Investigation of gas sensing property of zinc oxide thin films deposited by Sol–Gel method: effects of molarity and annealing temperature, Indian J. Phys. 95 (2021) 243–252.
19. G. Lu, S. Park, K. Yu, R.S. Ruoff, L.E. Ocola, D. Rosenmann, et al., Toward practical gas sensing with highly reduced graphene oxide: a new signal processing method to circumvent run to–run and device–to–device variations, ACS Nano 5 (2011) 1154–1164.
20. J. Li, W. Zhang, J. Sun, Enhanced NO_2 detection using hierarchical porous ZnO nanoflowers modified with grapheme, Ceramics International, 42 (2016) 9851–9857.

Figures

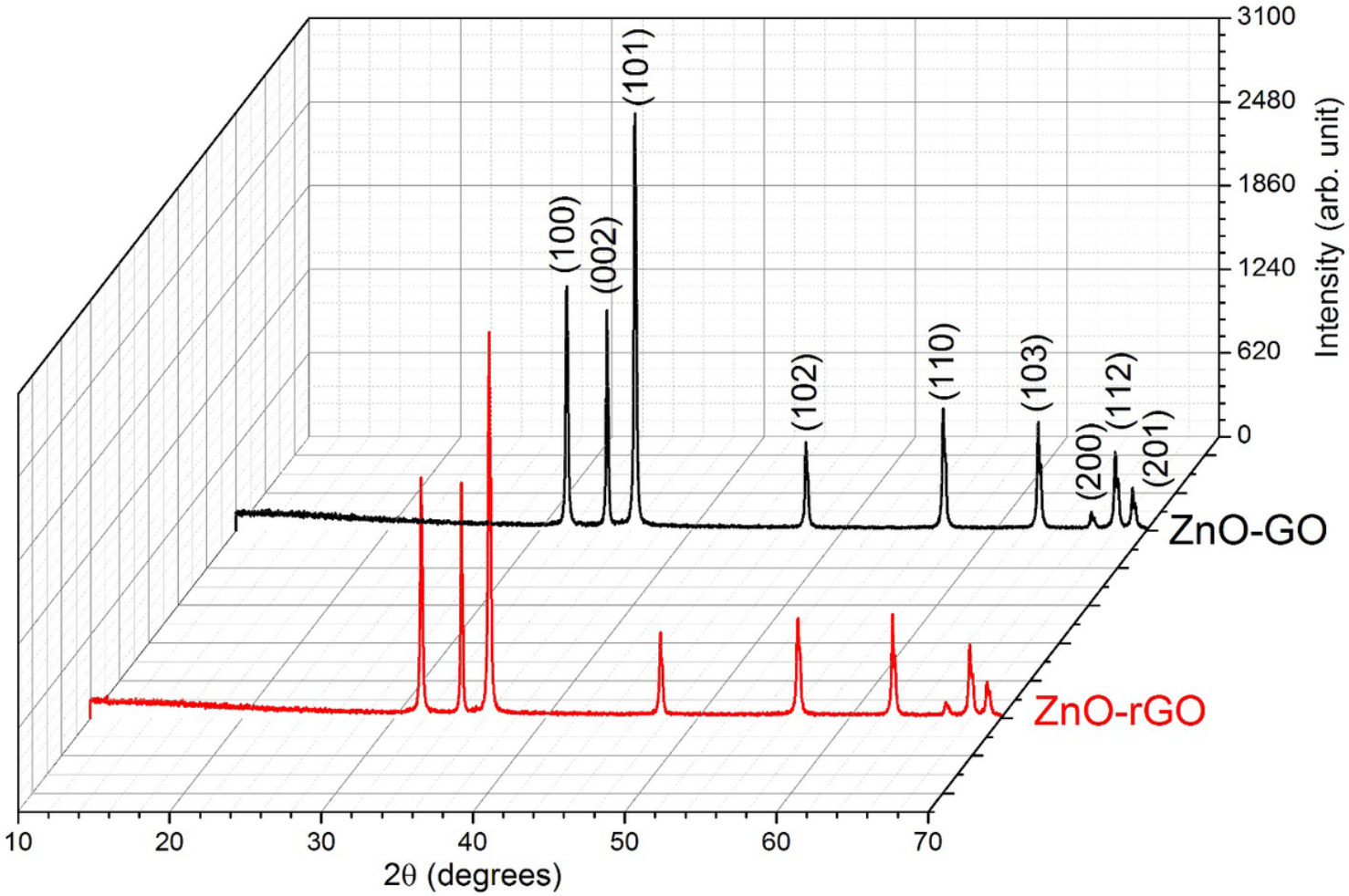

Figure 1

XRD patterns of the grown ZnO–GO and ZnO–rGO thin films.

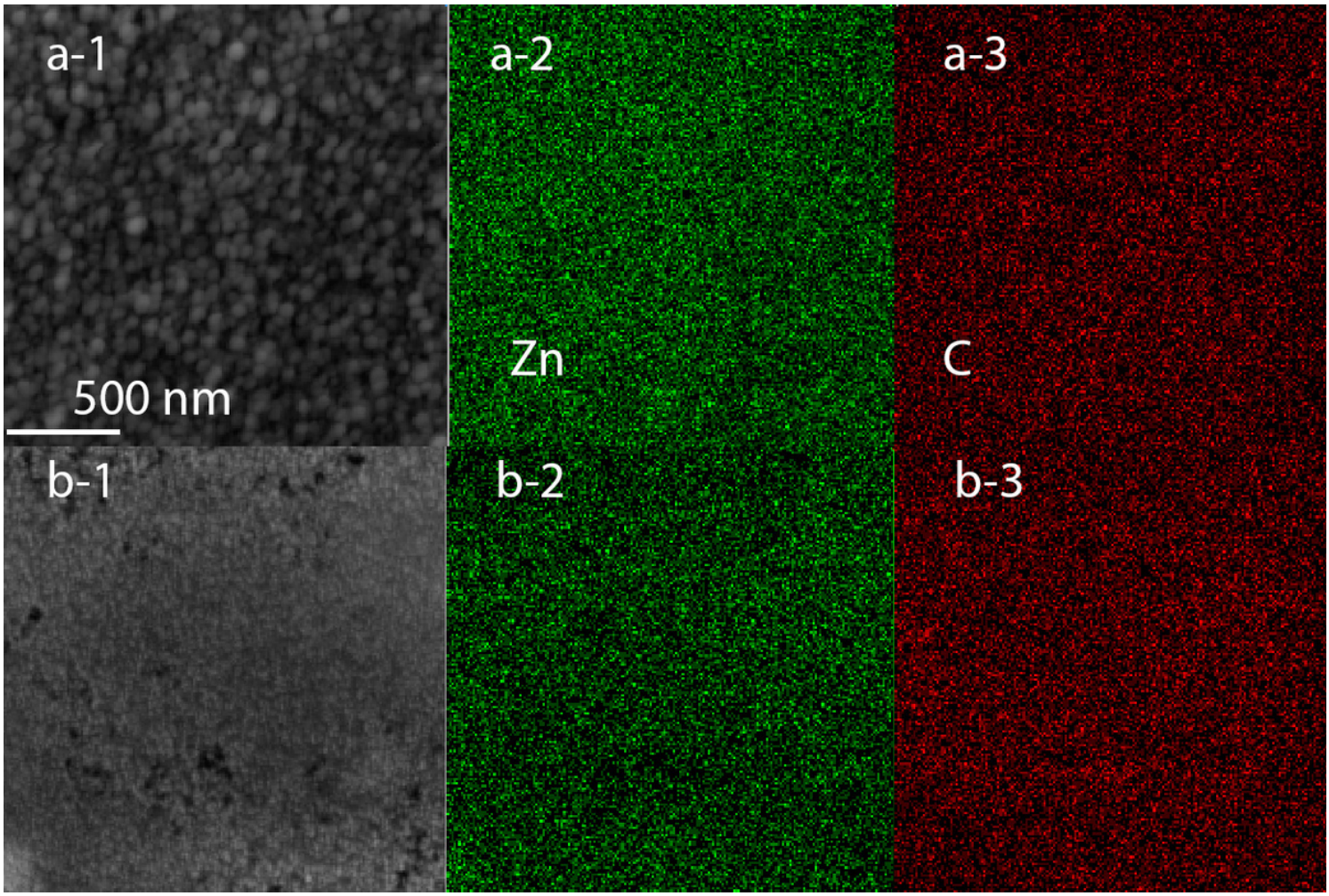

Figure 2

EDX mapping of elemental composition of (a) GO–ZnO and (b) rGO–ZnO thin films.

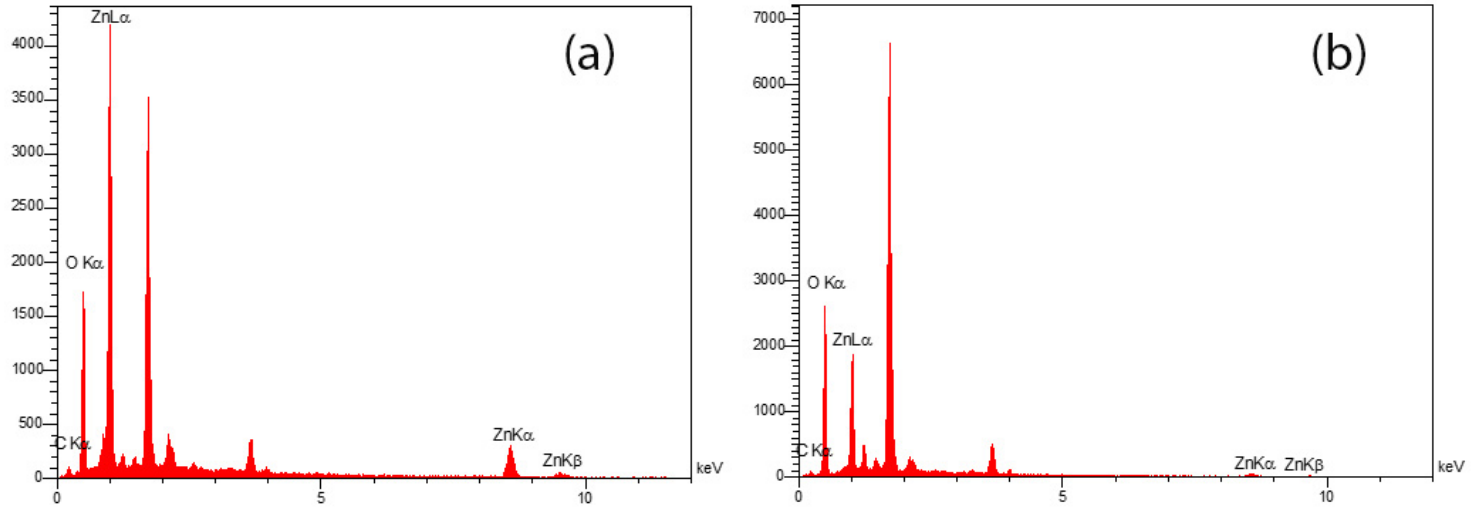

Figure 3

The EDX spectra for (a) GO–ZnO and (b) rGO–ZnO thin films.

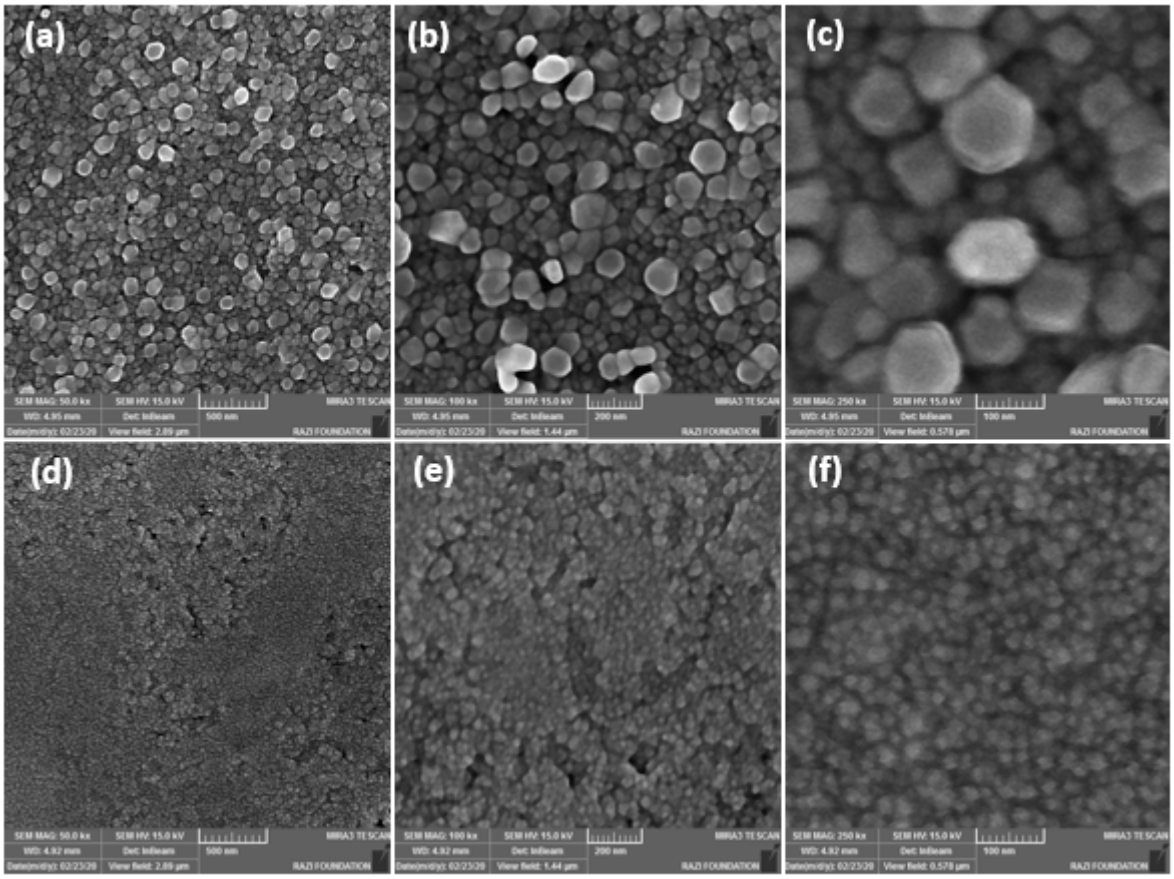

Figure 4

FESEM images of (a–c) GO–ZnO samples and (d–f) rGO–ZnO samples. These SEM images at different magnifications changed from 500nm to 100nm.

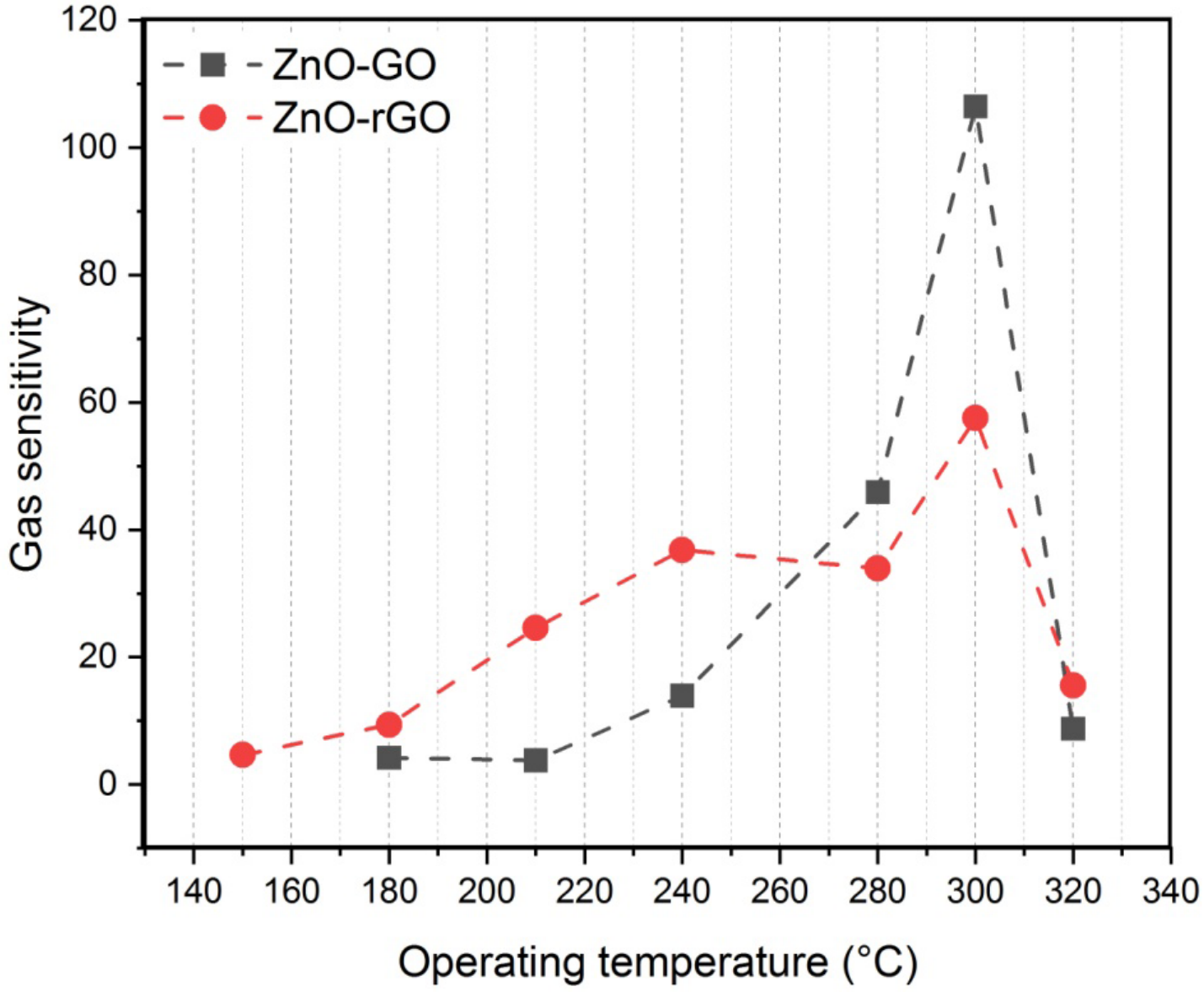

Figure 5

Gas sensitivity of the samples at different operating temperatures for GO and rGO–ZnO thin films (ethanol concentration 1200 ppm).

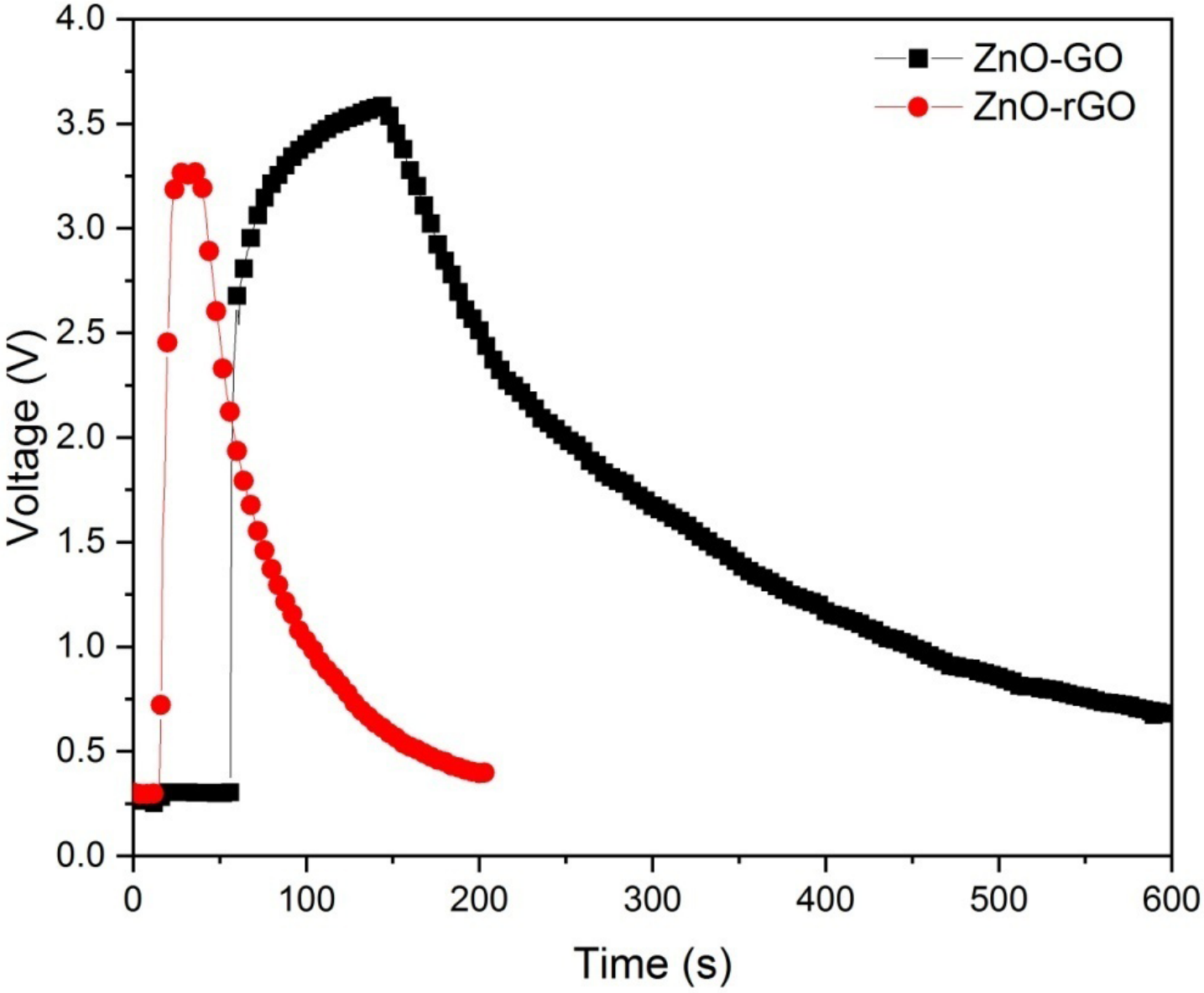

Figure 6

The real–time dynamic response of ZnO–GO and ZnO– rGO thin films upon exposure to 1200 ppm of ethanol at 300˚C

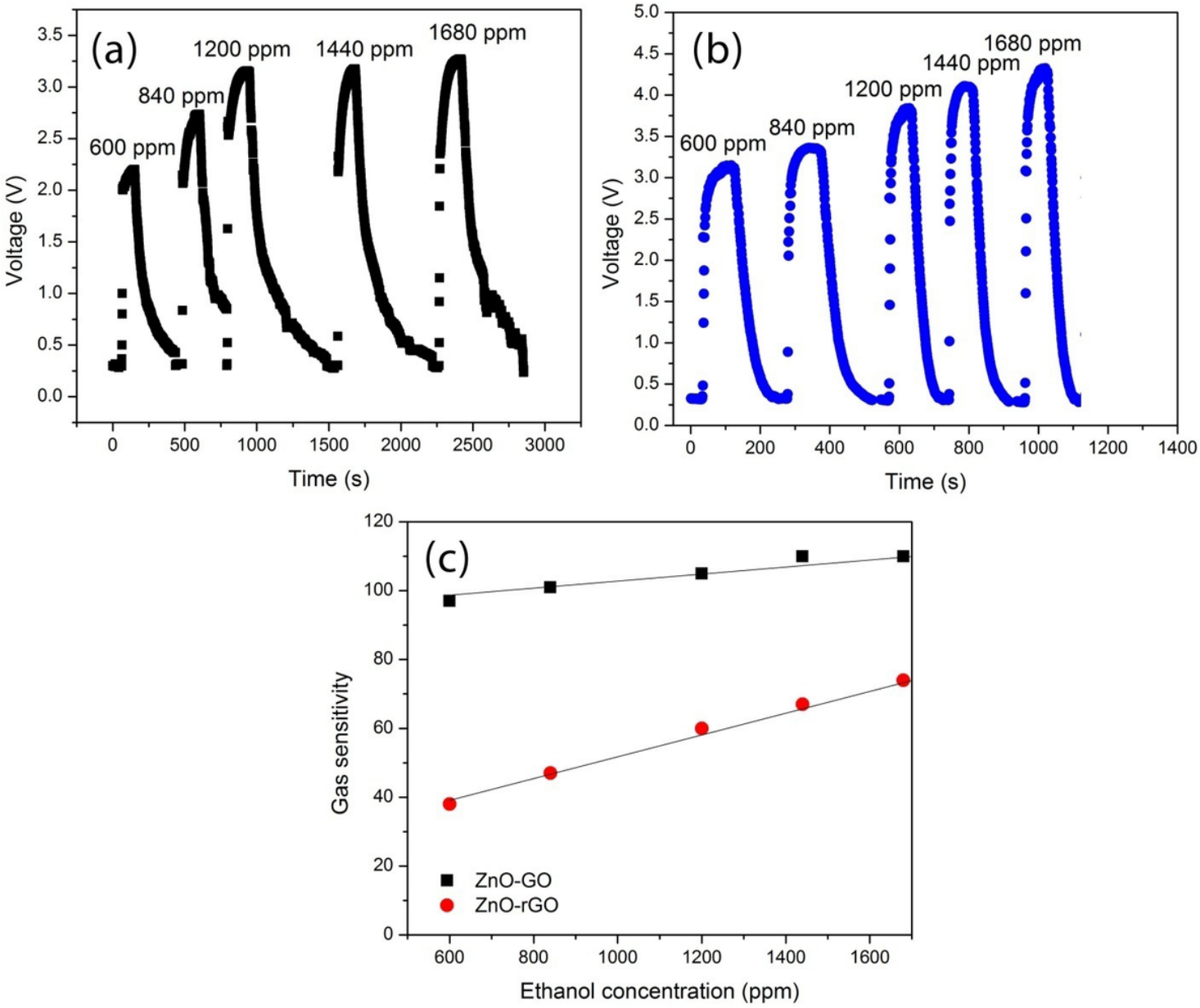

Figure 7

Response of (a) ZnO–GO and (b) ZnO–rGO based sensor and (c) the related sensitivity in different ethanol vapor concentrations.